

Magneto-optical spectroscopic scatterometry for analyzing patterned magnetic nanostructures

Roman Antos^a, Jan Mistrik^b, Tomuo Yamaguchi^b, Martin Veis^{c,d}, Eva Liskova^c, Stefan Visnovsky^c, Jaromir Pistora^e, Burkard Hillebrands^f, Sergej O. Demokritov^g, Takashi Kimura^h, and Yoshichika Otani^{a,h}

^a Frontier Research System, RIKEN, 2-1 Hirosawa, Wako, Saitama 351-0198, Japan

^b Research Institute of Electronics, Shizuoka University, 3-5-1 Johoku, Hamamatsu 432-8011, Japan

^c Charles University, Faculty of Mathematics and Physics, Ke Karlovu 5, 121 16 Praha 2, Czech Republic

^d Graduate School of Electronic Science and Technology, Shizuoka University, 3-5-1 Johoku, Hamamatsu 432-8561, Japan

^e VSB—Technical University of Ostrava, 17. listopadu 15, 708 33 Ostrava, Czech Republic

^f Department of Physics, University of Kaiserslautern, Erwin-Schrödinger-Strasse 56, 67663 Kaiserslautern, Germany

^g Institute of Applied Physics, Westfälische Wilhelms-University Münster, Corrensstrasse 2-4, 48149 Münster, Germany

^h Institute for Solid State Physics, University of Tokyo, Kashiwa, Chiba 277-8581, Japan

Methodology and selected applications of magneto-optical (MO) spectroscopic scatterometry (MOSS) are presented on various types of magnetic gratings made by lithographic patterning. Three types of theoretical models with different levels of accuracy are described in detail: a rigorous one, an analytical approximation, and a model mostly appropriate for real structures affected by line-edge roughness (LER). The MOSS approach, based on explaining diffracted MO Kerr effect measurements by simulations employing the mentioned models, is demonstrated as a technique highly sensitive to nanoscale features such as native oxide overlayers, as well as capable of determining the LER characteristic quantitatively. Further possibilities to study unsaturated magnetic structures and compositions of magnetic materials including imperfect deposition or aging processes are suggested.

Key words: magneto-optics, spectroscopy, scatterometry, grating, diffraction, Kerr effect, line-edge roughness

1. Introduction: The reason for working with magneto-optical spectroscopic scatterometry (MOSS)

Laterally patterned magnetic nanostructures are becoming of increasing interest owing to possible advantageous applications in magnetic and magneto-optical (MO) information storage media, light waveguiding and filtering tools, new metamaterials, etc. For those purposes, various nanoscale elements such as nanodots or nanowires with various shapes possessing particular spin structures are fabricated and investigated with respect to magnetic switching and dynamical processes.^{1,2)} The quality control of the lithographic fabrication is usually performed by conventional scanning probe techniques like atomic force microscopy (AFM) or scanning electron microscopy (SEM), usually inherited in the lithographer. Static micromagnetic properties such as equilibrium spin structures can be further analyzed by magnetic force microscopy³⁾ or spin-polarized scanning tunneling microscopy.⁴⁾ However, such techniques are expensive, cumbersome, and inappropriate for *in situ*, have low throughput, and are useless for monitoring the sub-nanosecond dynamical evolution of the spin structures.

Several monitoring techniques based on detecting the MO Kerr effect (MOKE) have been developed suggesting advantageous potentialities in both of the two areas mentioned, the quality control of lithography and monitoring the micromagnetic behavior. In the first

case, MO spectroscopy can serve as an additional scatterometric technique similar to purely optical spectroscopic ellipsometry (SE)⁵⁾ and reflectometry which are frequently used in industrial inspection. In the second case, usually single wavelength methods are applied such as the diffracted MOKE (D-MOKE)¹⁾ or microscopic MOKE (M-MOKE)⁶⁾ measurements. Both approaches provide approximate images of the geometrical distribution of magnetization. In the D-MOKE this information is distributed among the beams diffracted by the nanostructure's periodicity; the higher the diffraction order, the greater the sensitivity to the vicinity of the edges of magnetized elements. Thus, the D-MOKE is almost treated as the far-field discrete Fourier transform of a periodic magnetization function. On the other hand, the M-MOKE does not require the periodical arrangement of elements. In the wide-field mode,⁷⁾ the direct magnified image of a single element or a tiny array of elements is provided being sensitive to one chosen magnetization component. In the scanning mode,⁸⁾ the surface is scanned while the magnetization vector is determined at each point by analyzing asymmetries in the optical Fourier transform image.

The essential advantage of the both D- and M-MOKE measurements and the reason for their popularity is the simplicity of the data analysis, providing the direct or nearly direct magnetic image of the illuminated sample. However, these methods are affected by limitations of the optical imaging and by

imperfections of the investigated patterns. For instance, the periodicity of an analyzed structure comparable to the wavelength of detection light makes it almost impossible to record the sufficient number of higher diffraction orders for a proper D-MOKE analysis. Next, the M-MOKE is limited by the detection resolution, also affected by the nonzero wavelength and by the numerical aperture of the objective lens. And finally, the M-MOKE wide-field and scanned images are strongly affected by the so-called edge effects of the lateral patterning, i.e., the effects of internal diffraction by the edges of the patterned elements. The edge effects blur the recorded image and thus erase the information about magnetization near the vicinity of the magnetized elements. Particularly important edge effects affecting the MOKE approaches are the cross-polarization effect, observed when the angle of the incidence plane is oblique to the edges, and the depolarization effect, mainly caused by the line-edge roughness (LER) of the patterned elements. Note that LER has recently received high attention in AFM and SEM analyses, together with the linewidth roughness (LWR).^{9), 10)}

Clearly, the aim to keep using the MOKE techniques even beyond those limitations demands to evaluate those effects by a proper method which can securely distinguish between the magnetization response and the effects due to optical imaging and fabrication imperfections. In this paper we show that this demand is satisfied by MO spectroscopic scatterometry (MOSS) which can be applied as accurate quality control of lithographic manufacturing as well as a tool quantitatively determining the contribution of the LER, native oxide, and other effects to the MOKE response. Determining these contributions could be later utilized for extending the D- and M-MOKE analyses to higher resolution patterns.

2. Theoretical models for MO simulations

We briefly present the fundamental principles of modeling the MOKE parameters since they are important for understanding the MOSS methodology, especially for choosing an appropriate experimental configuration to monitor particular features. We apply three different models, the rigorous coupled-wave analysis (RCWA),¹¹⁾ the local modes method (LMM), and the reduced edge effect method (REEM) based on combining RCWA with LMM. We only use literature data of optical and MO parameters¹²⁾⁻¹⁶⁾ or their effective-medium approximations.¹⁷⁾

2.1 Rigorous coupled-wave analysis (RCWA)

We consider generally a two-dimensional (2D) grating patterned from an N -fold multilayer containing, for simplicity, uniformly polar-magnetized layers. The case of 1D grating can always be regarded as a limit. We write Maxwell's equations in an MO-anisotropic medium with 2D periodicity in the xy -plane as

$$\nabla \times \mathbf{E} = -i\mathbf{c}\mathbf{B}, \quad (1a)$$

$$\nabla \times \mathbf{c}\mathbf{B} = i\tilde{\epsilon}(x, y) \cdot \mathbf{E}, \quad (1b)$$

assuming solutions with the $\exp(i\omega t)$ time dependence. The space coordinates are factorized by $k_0 = 2\pi/\lambda$, where λ is the wavelength in vacuum. The 2D periodic permittivity tensor at polar magnetization established by the external magnetic field takes on the form

$$\tilde{\epsilon}(x, y) = \begin{bmatrix} \epsilon_{xx} & \epsilon_{xy} & 0 \\ \epsilon_{yx} & \epsilon_{yy} & 0 \\ 0 & 0 & \epsilon_{zz} \end{bmatrix}, \quad (2)$$

where $\epsilon_{yx} = -\epsilon_{xy}$ and $\epsilon_{yy} = \epsilon_{xx}$.

Eliminating the normal component of the electric field \mathbf{E} , we obtain a system of second-order differential equations for the tangential components, i.e.,

$$\begin{pmatrix} \hat{C}_{xx} & \hat{C}_{xy} \\ \hat{C}_{yx} & \hat{C}_{yy} \end{pmatrix} \begin{bmatrix} E_x \\ E_y \end{bmatrix} = -\partial_z^2 \begin{bmatrix} E_x \\ E_y \end{bmatrix}, \quad (3)$$

where

$$\hat{C}_{jk} E_k = \left[\epsilon_{jk} - \partial_j \partial_k + \delta_{jk} (\partial_x^2 + \partial_y^2) + \partial_j \frac{1}{\epsilon_{zz}} (\partial_x \epsilon_{xk} + \partial_y \epsilon_{yk}) \right] E_k, \quad (4)$$

with j and k representing any of x and y , respectively, and with δ_{jk} denoting the Kronecker symbol.

In the frame of RCWA all the electric and magnetic fields are expanded into pseudo-Fourier series whose coefficients become elements of column vectors representing light states. Then the Fourier coefficients of the periodic permittivity function of the grating's texturing are used to construct matrices acting on the light state vectors. Thus the wave propagation equation and the requirement for the continuity of tangential field components are reformulated to matrix formulae that are solved by linear-algebraic techniques. Thus, Eq. (3) becomes a matrix equation for eigenmodes,

$$\mathbf{C}\mathbf{e}_\alpha = \mu_\alpha \mathbf{e}_\alpha, \quad (5)$$

or, alternatively,

$$\mathbf{C}\mathbf{T} = \mathbf{T}\mathbf{D}, \quad (6)$$

where \mathbf{T} is a diagonalizer of \mathbf{C} . Now we can write the propagation matrix relating the modes in two planes $z = z_0$ and $z = z_1$, i.e.,

$$\mathbf{P} = \mathbf{T}\mathbf{P}_{\text{diag}}\mathbf{T}^{-1}, \quad (7)$$

where \mathbf{P}_{diag} is a diagonal matrix composed of $\exp[i\lambda(z_1 - z_0)s_\alpha]$ with $s_\alpha = \pm(\mu_\alpha)^{1/2}$. The sign of the complex square root is chosen in the manner to have the physical meaning. Similarly, we derive a formula for the tangential magnetic field components,

$$\partial_z \begin{bmatrix} cB_y \\ -cB_x \end{bmatrix} = \begin{pmatrix} \hat{D}_{xx} & \hat{D}_{xy} \\ \hat{D}_{yx} & \hat{D}_{yy} \end{pmatrix} \begin{bmatrix} E_x \\ E_y \end{bmatrix}, \quad (8)$$

where

$$\hat{D}_{jk} E_k = [\epsilon_{jk} - \hat{c}_j \hat{c}_k + \delta_{jk} (\partial_x^2 + \partial_y^2)] E_k, \quad (9)$$

from which the matrix formula immediately follows,

$$\tilde{\mathbf{b}} = \tilde{\mathbf{D}}\mathbf{e} = \mathbf{D}\mathbf{T}^{-1}\mathbf{T}^{-1}\mathbf{e}, \quad (10)$$

with \mathbf{S} being a diagonal matrix composed of s_α .

From the continuity of \mathbf{e} and $\tilde{\mathbf{b}}$ on the interface between two adjacent media J and $J+1$, we obtain

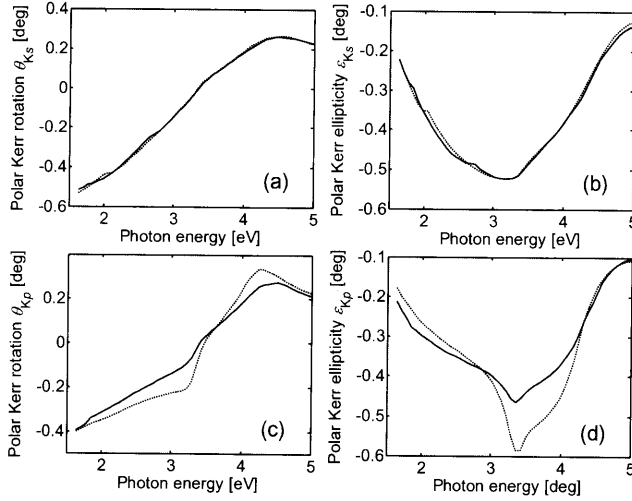


Fig. 1 RCWA simulations of the Polar Kerr effect in the -1 st diffraction order for s - (a,b) and p -polarized (c,d) light incident on 15 nm thick Permalloy wires on an Si substrate under 30° of incidence. The full (dotted) curves correspond to the period of 900 (1200) nm and the wire linewidth of 600 (800) nm.

reflection and transmission matrices

$$\mathbf{R}^{J,J+1} = -\left[1 + (\tilde{\mathbf{D}}^{(J+1)})^{-1} \tilde{\mathbf{D}}^{(J)}\right]^{-1} \left[1 - (\tilde{\mathbf{D}}^{(J+1)})^{-1} \tilde{\mathbf{D}}^{(J)}\right], \quad (11a)$$

$$\mathbf{T}^{J,J+1} = 1 + \mathbf{R}^{J,J+1}, \quad (11b)$$

relating the reflected and transmitted mode amplitudes of all the diffraction orders to the mode incident to that interface, with 1 being the unit matrix. We start from $\mathbf{R}^{0,1}$ and $\mathbf{T}^{0,1}$ and proceed iteratively until we reach $\mathbf{R}^{0,N+1}$ and $\mathbf{T}^{0,N+1}$ using the recursive algorithm

$$\mathbf{R}^{0,J+1} = \mathbf{R}^{0,J} + \mathbf{T}^{J,0} \mathbf{P}^{(J)} \mathbf{R}^{J,J+1} \left(1 - \mathbf{Q}^{(J)}\right)^{-1} \mathbf{P}^{(J)} \mathbf{T}^{0,1}, \quad (12a)$$

$$\mathbf{T}^{0,J+1} = \mathbf{T}^{J,J+1} \left(1 - \mathbf{Q}^{(J)}\right)^{-1} \mathbf{P}^{(J)} \mathbf{T}^{0,1}, \quad (12b)$$

with $\mathbf{Q}^{(J)} = \mathbf{P}^{(J)} \mathbf{R}^{(J,J-1)} \mathbf{P}^{(J-1)} \mathbf{R}^{(J,J+1)}$.

Finally, we obtain the amplitude reflection coefficients $r_{ss}^{(n)}$, $r_{sp}^{(n)}$, $r_{ps}^{(n)}$, and $r_{pp}^{(n)}$ for each n th diffraction order, obtained as the elements of the central columns of the subblocks of $\mathbf{R}^{0,N+1}$, and similarly for transmission. Using the reflection coefficients we calculate the MOKE ellipsometric angles, the Kerr rotation θ and ellipticity ε , as

$$\theta_{Ks}^{(n)} - i\varepsilon_{Ks}^{(n)} \approx r_{ps}^{(n)} / r_{ss}^{(n)}, \quad (13a)$$

$$\theta_{Kp}^{(n)} - i\varepsilon_{Kp}^{(n)} \approx -r_{sp}^{(n)} / r_{pp}^{(n)}, \quad (13b)$$

(in each n th diffraction order) for the s and p polarized incident light, respectively, provided that the ellipsometric angles are small.

An example of RCWA calculation in the -1 st diffraction order is displayed in Fig. 1 for two examples of periods, but with equal ratios of the wire linewidth to the period. This allows one to display the dependence of the MOKE response partly on the lateral distribution of the wires' area and partly on the effects of the wires'

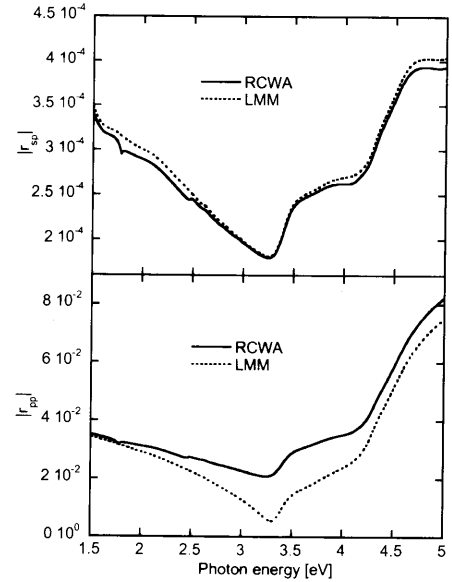


Fig. 2 Comparison of RCWA (solid curves) and LMM (dotted curves) simulations of magnitudes of -1 st order diffracted reflectance coefficients $r_{sp}^{(-1)}$ and $r_{pp}^{(-1)}$ for $\text{Cr}_2\text{O}_3(2 \text{ nm})/\text{NiFe}(11 \text{ nm})$ wires on an $\text{SiO}_2(2 \text{ nm})/\text{Si}$ substrate with the period of 900 nm and wire linewidth of 536 nm.

edges. It is clearly visible that the MOKE response with p polarized incident light is significantly more sensitive to the size of the period, and hence also to these effects [Fig. 1(c,d)]. This sensitivity is realized via the denominator in Eq. (13b). To distinguish between the lateral distribution response and the edge effects, we below develop two other theoretical approaches.

2.2 Local modes method (LMM)

LMM is an approximate analytical method based on the far-field Fourier analysis of the amplitude reflectance distribution where the reflection coefficients are at each point of the grating's surface evaluated by assuming local lateral uniformity with multilayer-like structure. This method, derived for treating shallow diffraction patterns, entirely neglects the diffraction effects of the edges of patterned elements, and is universally adopted by D- and M-MOKE analyses under various nomenclatures.

As the result of the far-field Fourier transform, the amplitude reflectance coefficients in the specular reflection do not depend on the periodical arrangement, but are just weighted functions of the reflectances of the two alternating media,

$$r_{jk}^{(0)} = w r_{I,jk} + (1-w) r_{II,jk}, \quad (14a)$$

where $r_{I,jk}$ and $r_{II,jk}$ represent the amplitude reflectance coefficients corresponding to a magnetic element (non-etched medium) and to a space between elements (etched medium including the air gap), respectively, $w = A/L$ denotes the filling factor of the pattern (ratio of the element area A to the period area L), and j, k represent any of the s and p polarizations.

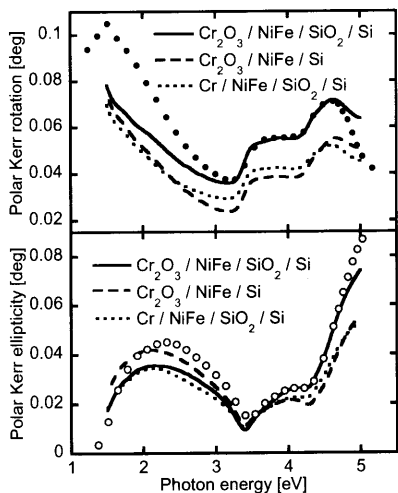


Fig. 3 The specular MOKE spectra measured on Sample 2 (circles) and compared with LMM simulations employing different thicknesses of the capping and substrate native oxide layers: $t(\text{Cr}_2\text{O}_3) = 2$ nm and $t(\text{SiO}_2) = 3$ nm (full curves), $t(\text{Cr}_2\text{O}_3) = 2$ nm and $t(\text{SiO}_2) = 0$ (dashed curves), $t(\text{Cr}) = 2$ nm and $t(\text{SiO}_2) = 3$ nm (dotted curves).

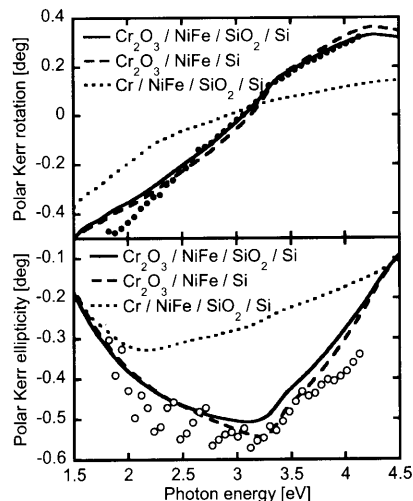


Fig. 4 The -1 st order MOKE spectra measured on Sample 2 (circles) and compared with LMM simulations employing different thicknesses of the capping and substrate native oxide layers: $t(\text{Cr}_2\text{O}_3) = 2$ nm and $t(\text{SiO}_2) = 3$ nm (full curves), $t(\text{Cr}_2\text{O}_3) = 2$ nm and $t(\text{SiO}_2) = 0$ (dashed curves), $t(\text{Cr}) = 2$ nm and $t(\text{SiO}_2) = 3$ nm (dotted curves).

Of course, higher diffraction orders depend also on the periodical arrangement. If we assume a simple 1D array of periodic nanowires with the direction of periodicity lying in the plane of incidence, we obtain

$$r_{jk}^{(n \neq 0)} = \frac{i}{2\pi n} (r_{I,jk} - r_{II,jk}) (1 - e^{2\pi i n w}), \quad (14b)$$

which depends on the period only via the filling factor.

To show more concrete evidence of the sensitivity to the edge effects, Fig. 2 demonstrates a comparison of RCWA and LMM simulations corresponding to an experimental example discussed below. As clearly visible, only r_{pp} exhibits differences suggesting sensitivity to the edge effects. Analogous simulations of r_{ss} and r_{ps} do not reveal such sensitivity.

2.3 Reduced edge effects method (REEM)

If we evaluate the response of an ideal structure as the exact RCWA calculation and rewrite it into the form

$$r_{pp}^{\text{ideal}} = r_{pp}^{\text{LMM}} + (r_{pp}^{\text{RCWA}} - r_{pp}^{\text{LMM}}), \quad (15)$$

then the value in the parentheses is the error of LMM with respect to rigorous calculation. This error can just be identified with the effect of pattern edges. In reality the part of this effect is reduced due to LER. The reduction can be taken into account by a slightly generalized formula

$$r_{pp}^{\text{REEM}} = r_{pp}^{\text{LMM}} + \eta(\lambda) (r_{pp}^{\text{RCWA}} - r_{pp}^{\text{LMM}}), \quad (16)$$

yielding a more realistic value. Here the effect of edges written in the parentheses is reduced by the factor η taking on values assumed between 0 and 1. We refer to the η -factor as the LER parameter, being $\eta = 1$ in the case of ideal, regular edges, or $\eta = 0$ when no edge effects are observed. Although the LER parameter is generally assumed to depend on the wavelength, in our experimental example below no dependence is observed.

3. Experimental applications of MOSS

We apply MOSS to analyze arrays of periodic 10 nm thick Permalloy wires deposited on Si substrates with periodicities of nearly 1000 nm and with protection by a top 2 nm thick Cr capping layer. Three samples with different periods and wire linewidths were fabricated by means of electron beam lithography combined with ion beam etching. The grating parameters were verified by AFM, which allowed minimizing the number of parameters to be determined by MOKE. The geometrical parameters extracted from AFM pictures are summarized in Table 1.

Table 1 Description of the samples

Sample	Period	Linewidth	Thickness(NiFe)
1	900 nm	536 nm	11 nm
2	910 nm	700 nm	12 nm
3	970 nm	680 nm	10 nm

The MOKE experiments were performed with an MO spectroscopic ellipsometer employing the azimuth modulation and compensation technique. The samples were set up with applied out-of-plane magnetic field of 1.4 T, sufficient to saturate the polar magnetization. The MO response in the specular mode was measured in incidence of 7° in the spectral range of 1.3–5.1 eV for both the s - and p -polarized incident beams without revealing differences. The reflection angles of higher diffraction orders are wavelength dependent; therefore, a special arrangement was adopted to measure the MOKE in the -1 st diffraction order. The angle between the incident and reflected beams was fixed to 20° , with

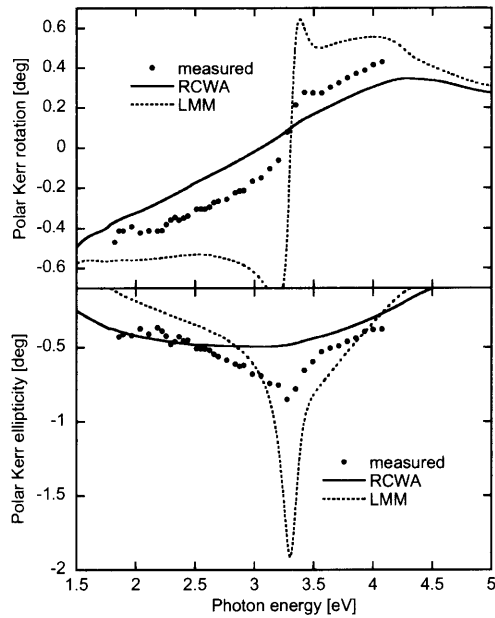


Fig. 5 LMM and RCWA simulations of the -1 st diffraction order MOKE with p -polarized incident light compared with experimental data obtained on Sample 1.

the sample free to rotate about the axis parallel to the wires, while the wavelength was swept. The position of the beam spot on the detector could not be kept completely fixed with the changing wavelength, which produced artificial jumps in the measured spectra. For this reason, from the experimental data obtained on all the three samples we only present those with tiniest jumps in order to demonstrate the most reliable analyses.

We distinguish between two different MOSS analyses. First, the application of s -polarized incident light enables us to detect the presence and thickness of native oxide overlayers developed both on the top of the Cr capping and on the naked Si. We present this analysis obtained on Sample 2 because here the measurement with s -polarized incident light was affected by the smallest artificial jumps mentioned above. According to the considerable differences among the simulation curves in Fig. 3, the specular (0th order diffracted) MOKE possesses ultrahigh sensitivity to the nanoscale native oxides. However, both the top native Cr_2O_3 overlayer and the SiO_2 interlayer exhibit similar trends, and hence the diffracted MOKE in the -1 st order becomes essential for distinguishing between the two oxides, as obvious from Fig. 4. Here the account for the completely oxidized capping layer [$t(\text{Cr}_2\text{O}_3) = 2$ nm] remarkably improves the agreement with the experiment. On the other hand, the -1 st order diffracted MOKE is less sensitive to $t(\text{SiO}_2)$. The explanation can be found in Eq. (14b), because the contributions of SiO_2 to both $r_{I,jk}$ and $r_{II,jk}$ are comparable making the sensitivity of their difference

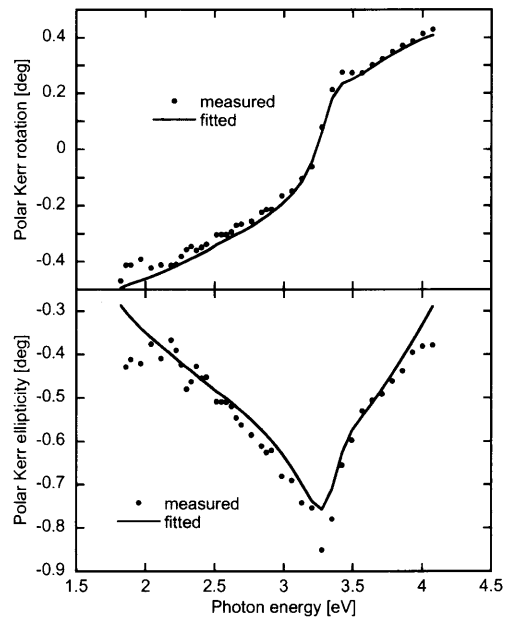


Fig. 6 REEM calculation fitted to the experimental data from Fig. 5.

weak to $t(\text{SiO}_2)$. This fact is essential for the selective account for the effect of the native oxides and thus manifests the uniqueness of the proposed technique even without simultaneous analyses of reference samples.

In Figs. 3 and 4 we have only shown LMM simulations since those yielded by RCWA were nearly identical. The agreement between LMM and RCWA simulations does not occur when p -polarized incident light is applied, which we utilize in the second MOSS analysis. Concretely, the application of p -polarized incident light in a -1 st diffraction order configuration where r_{pp} takes on small values enables us to detect LER with remarkable sensitivity. Due to the jumps mentioned above, for p -polarized incident light appearing more significantly on Sample 2, we present this analysis performed on Sample 1. The effect of ideal edges can be seen from Fig. 5, where we compare the RCWA and LMM calculations, none of which correctly follows the experimental data. On the other hand, the application of the REEM yields remarkable agreement with the measurement (Fig. 6), provided we have fitted the LER parameter $\eta = 0.53$ defined by Eq. (16). As mentioned above, taking a constant value independent of wavelength was sufficient. The same fitting procedure performed on Sample 2 yielded $\eta = 0.70$, suggesting that Sample 2 is of higher quality. Qualitative comparison of the pattern quality of the both samples can be done by viewing their AFM images shown in Fig. 7, where such difference is indeed evident.

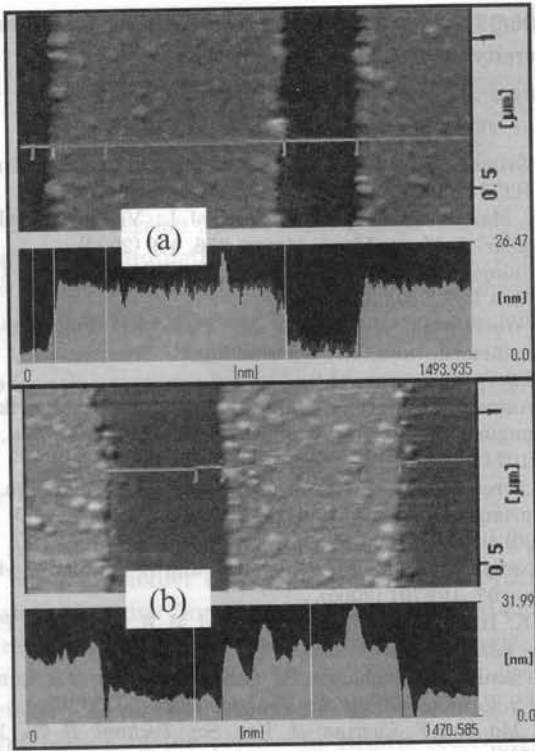


Fig. 7 Top-viewed and cross-sectional atomic force micrographs of Samples 1 (b) and 2 (a).

Analogously we apply MOSS using our three models to two other sets of samples. First of them is a partially etched uncovered Py(32 nm)/Si structure with the period of 1000 nm and wire linewidth of 307 nm. The nearly-normal-incidence specular MOKE response of a chosen sample etched up to 24 nm of depth is displayed in Fig. 8(a). Unfortunately, there is not available literature permittivity data of oxide formed

from Permalloy, so that a possible native oxide overlayer had to be excluded from calculation. Moreover, this measurement was done with applied out-of-plane magnetic field of only 0.4 T which did not probably saturate the sample completely. Both effects could therefore create the discrepancies visible in parts of the presented spectral dependences.

The second set consists of partially oxidized Ni wires deposited on a thermally oxidized system SiO₂(500 nm)/Si. The nearly-normal specular MOKE response of a sample with the wire thickness of about 40 nm is displayed in Fig. 8(b). Here the deep SiO₂ interlayer entails significant interference effects which considerably increase the sensitivity of the approach. The reasonable correspondence between simulation and experiment visible in the figure was achieved by assuming that Ni was partially oxidized already during the deposition process. The composition of the Ni₅₂(NiO)₄₈ structure uniform within depth was determined by a fitting procedure involving both MOKE and purely optical SE data. Moreover, the MO effect had to be reduced down to 25 %, which cannot be explained by unsaturated polar magnetization. The most probable explanation assumes that a possible nanocrystalline character of the Ni₅₂(NiO)₄₈ structure reduces the MO constants of the system as the whole.

4. Conclusions

We have demonstrated MOSS as a highly sensitive and precise method of observing various geometrical and material characteristics of laterally patterned periodic nanostructures. Choosing certain measurement configurations enabled us to detect particular structure properties. By employing s-polarized incident light we

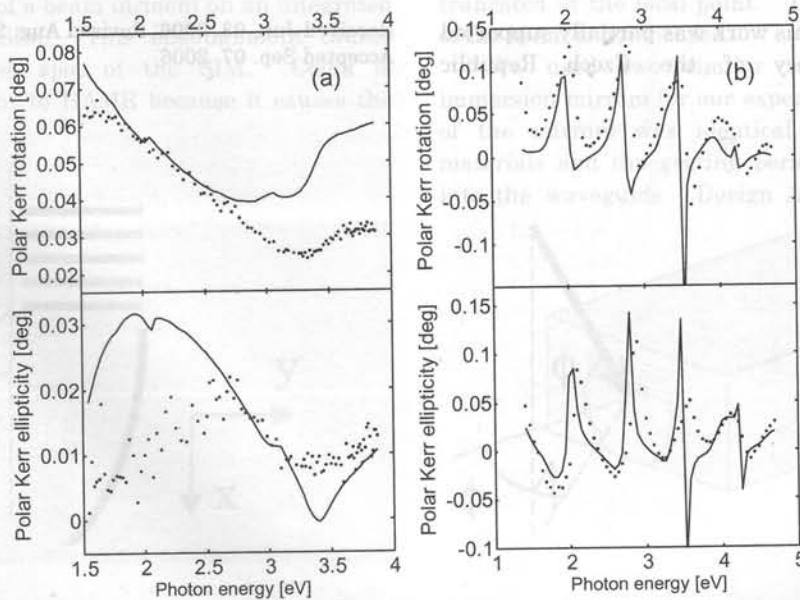


Fig. 8 Specular MOKE spectra with nearly-normal incidence obtained on a partially etched NiFe(32)/Si structure (a) and Ni wires on a SiO₂(500 nm)/Si structure (b). Experimental data (points) are compared with RCWA simulations (curves).

were capable to monitor the presence and thickness of nanoscale native oxides: by employing p -polarized incident light we evaluated the LER parameter.

The essential advantage of the chosen configurations is the uniqueness of what they detect. For instance, the LER parameter does not affect the measurement with s -polarized incident light. Similarly, by examining the sensitivity of particular diffracted beams to particular structure features we have demonstrated the uniqueness of determining the native oxides developed either on the top of the structure's capping or on the naked substrate.

For the analysis of the experimental data we have described three theoretical models, a rigorous one, an analytical approximation, and a method combining both and employing an additional parameter. We have shown that choosing a model of a particular level of accuracy does not necessarily mean better or worse agreement with measurement. Instead, particular physical properties can be explained by adjusting the value of accuracy (proportional here to the LER parameter).

We have also suggested a possibility to employ MOSS for observing other properties such as unsaturated magnetization, material composition, or particular crystalline properties caused by imperfect deposition processes. The approach can obviously be arranged for investigating arbitrary surface material changes due to aging or thermal treating as well as for LER or LWR control in industrial production. After an appropriate generalization, the theoretical model demonstrated here could be also applied to binary magnetic gratings with arbitrary magnetization distribution such as arrays of dots with vortex spin structures.

Acknowledgements This work was partially supported by the Grant Agency of the Czech Republic

(202/06/0531) and the Grant Agency of Charles University (314/2004/B - FYZ/MFF).

References

- 1) M. Grimsditch and P. Vavassori: *J. Phys.: Condens. Matter*, **16**, R275 (2004).
- 2) J. I. Martin, J. Nogues, K. Liu, J. L. Vicent, and I. K. Schuller: *J. Magn. Magn. Mater.*, **256**, 449 (2003).
- 3) T. Shinjo, T. Okuno, R. Hassdorf, K. Shigeto, and T. Ono: *Science*, **289**, 930 (2000).
- 4) A. Wachowiak, J. Wiebe, M. Bode, O. Pietzsch, M. Morgenstern, and R. Wiesendanger: *Science*, **298**, 577 (2002).
- 5) R. Antos, J. Pistora, I. Ohlidal, K. Postava, J. Mistrik, T. Yamaguchi, S. Visnovsky, and M. Horie: *J. Appl. Phys.*, **97**, 053107 (2005).
- 6) Y. Acremann, C. H. Back, M. Buess, O. Portmann, A. Vaterlaus, D. Pescia, and H. Melchior: *Science*, **290**, 492 (2000).
- 7) A. Neudert, J. McCord, R. Schafer, and L. Schultz: *J. Appl. Phys.*, **97**, 10E701 (2005).
- 8) W. K. Hiebert, A. Stankiewicz, and M. R. Freeman: *Phys. Rev. Lett.*, **79**, 1134 (1997).
- 9) J. Thiault, J. Foucher, J. H. Tortai, O. Joubert, S. Landis, and S. Pauliac: *J. Vac. Sci. Technol. B*, **23**, 3075 (2005).
- 10) Y. Ma and F. Cerrina: *J. Vac. Sci. Technol. B*, **23**, 1096 (2005).
- 11) S. Visnovsky and K. Yasumoto: *Czech. J. Phys.*, **51**, 229 (2001).
- 12) G. Neuber, R. Rauer, J. Kunze, T. Korn, C. Pels, G. Meier, U. Merkt, J. Backstrom, and M. Rubhausen: *Appl. Phys. Lett.*, **83**, 4509 (2003).
- 13) P. Hones, M. Diserens, and F. Levy: *Surf. Coat. Tech.*, **120-121**, 277 (1999).
- 14) *Handbook of Optical Constants of Solids*, E. D. Palik ed., (Academic, Tokyo, 1998).
- 15) S. Visnovsky, V. Parizek, M. Nyvlt, P. Kielar, V. Prosser, and R. Krishnan: *J. Magn. Magn. Mater.*, **127**, 135 (1993).
- 16) R. J. Powel and W. E. Spicer: *Phys. Rev. B*, **2**, 2182 (1970).
- 17) D. Stroud: *Phys. Rev. B*, **12**, 3368 (1975).

Received Jun. 03, 2006; Revised Aug. 23, 2006;
Accepted Sep. 07, 2006